Prepared for publication as an Article in *Analytical Chemistry*

Label-free, non-optical readout of bead-based immunoassays with and without electrokinetic preconcentration

Sommer Osman,† Echo L. Claus,† Robbyn K. Anand*

The Department of Chemistry, Iowa State University, 2415 Osborn Drive, 1605 Gilman Hall, Ames, Iowa 50011-1021, United States.

†These authors contributed equally.

*To whom correspondence should be addressed

E-mail: rkanand@iastate.edu

Submitted: November 12, 2022

Abstract

In this article, we report a microfluidic bead-based lateral flow immunoassay (LFIA) with a novel sensing mechanism for label-free, non-optical detection of protein binding. This device comprises two packed beds of microbeads: the first, bioconjugated microbeads that serve as a test line, and second, a 3D electrode for sensing. As the protein target binds the bioconjugated microbeads, a shift in ionic conductivity across the bioconjugated beads is produced and can be directly measured at the surface of the 3D electrode by obtaining current-voltage curves (CVCs) before and after incubation of the analyte. We use a model antigen, rabbit IgG, for quantitative evaluation of this sensor, obtaining a limit-of-detection (LOD) of 31 nM for the LFIA. We demonstrate this device can be used to measure binding kinetics, exhibiting a rapid (< 3 min) increase in signal after introduction of the analyte, and an exponential decay in signal after replacing the sample with buffer only. To improve the LOD of our system, we implement an electrokinetic preconcentration technique, faradaic ion concentration polarization (fICP), to increase the local concentration of antigen available during binding as well as the time the antigen interacts with the test line. Our results indicate that this enrichment-enhanced assay (fICP-LFIA) has an LOD of 370 pM, an 84-fold improvement over the LFIA, and a 4-fold improvement in sensitivity. We anticipate this device can be readily adapted for point-of-care (POC) diagnostics and translated to any desired protein target by simply modifying the biorecognition agent on these off-the-shelf microbeads.

Keywords: *biosensors, microfluidics, lateral flow immunoassay, ion concentration polarization, point-of-care diagnostics*

TOC Graphic

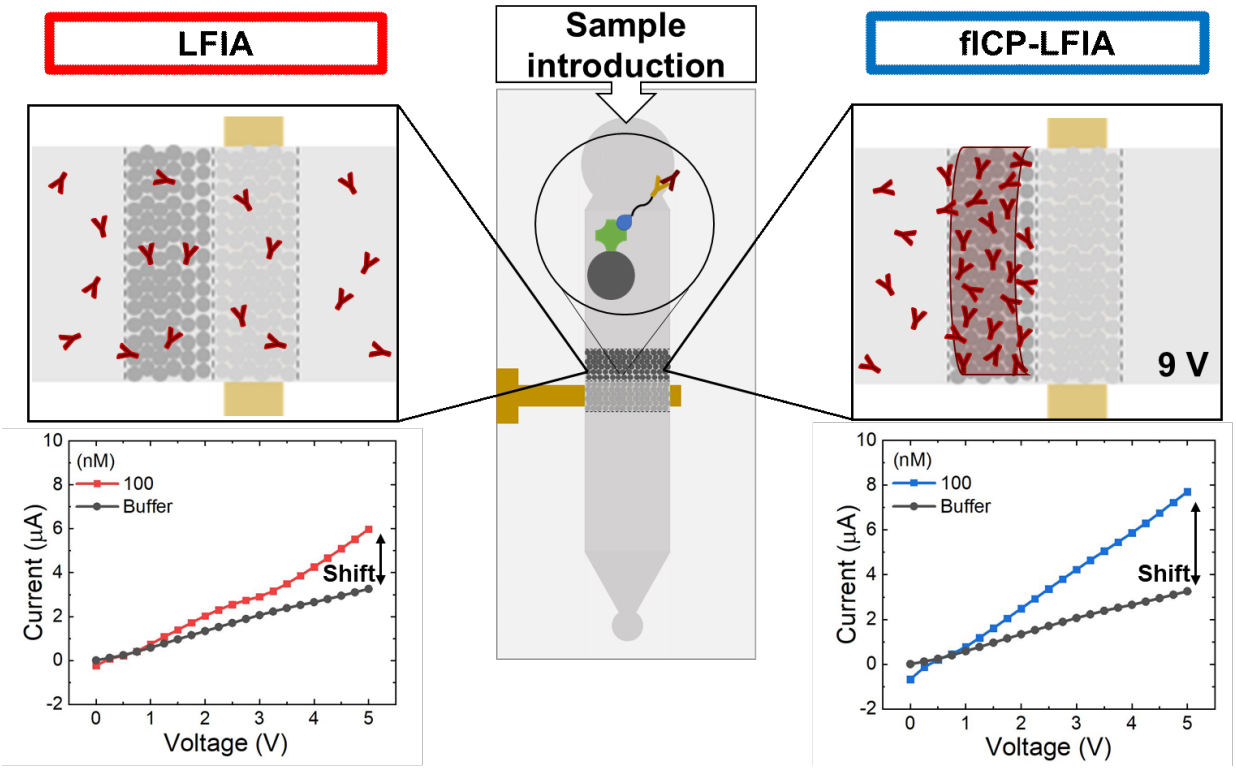
LFIA
Sample introduction
fICP-LFIA
9 V
(nM)
100
Buffer
Shift
Current (μA)
Voltage (V)
(nM)
100
Buffer
Shift
Current (μA)
Voltage (V)

Introduction

The recent pandemic exposed a critical gap in point-of-care (POC) diagnostics, where there is a need for more rapid, sensitive, and deliverable assays.[1] POC immunoassays focus specifically on protein sensing at the location of the patient, moving testing from large laboratories and into the hands of doctors and patients.[2] One of the best examples of this is the lateral flow immunoassay (LFIA), such as the widely used at-home pregnancy test.[3,4] While LFIAs are advantageous in that they should not require any special equipment to operate, they typically provide qualitative results, without indication of the amount of antigen in the sample, which can be key for ascertaining the patient's condition.

Microfluidic and lab-on-chip technologies are widely used for quantitative sample analysis. One significant innovation for microfluidic LFIAs has been the incorporation of bioconjugated beads for localization of the probe. Many bead-based immunoassays have been shown to enhance assay sensitivity and are used due to the high surface-to-volume ratio of the beads.[5] Another advancement in the field of immunoassays has been the integration of electrokinetic enrichment to improve limits-of-detection (LOD) and sensitivity. By adding a preconcentration step, researchers can increase the local concentration of antigen during the assay and thereby, increase the occurrence of binding events for antigen-antibody complexes.[5,6] Preconcentration in the context of LFIAs has been applied to microfluidic devices,[7,8] paper-based devices,[9,10] and microbead assays.[6,11–15] A number of electrokinetic techniques for sample preconcentration have been used in biosensing, such as ion concentration polarization (ICP), isotachophoresis (ITP), and field-amplified stacking (FASS).[7,13] It should be noted that ICP is advantageous among these methods due to its achievement of high enrichment factors without the

need for specialized buffers and its ability to generate and sustain for long periods the electric field gradient required for focusing.[7]

ICP is the simultaneous enrichment and depletion of ions at the opposite ends of a nanojunction with voltage application. In the presence of opposing fluid flow, ICP can be used to focus charged analytes along a steep electric field gradient generated by the high resistivity of the ion depletion zone (IDZ).[7,8,16] Researchers have leveraged this phenomenon to interface ICP with bead-based immunoassays for greater sensitivity. Wang et al. developed a nanofluidic preconcentrator that improved the sensitivity of a bead-based immunoassay, more than 500-fold, by increasing the concentration of antigen available during the LFIA and driving the reaction towards the forward (bound) direction.[6] This device was modified for the detection of notable cancer biomarkers by performing ELISA off-chip, with the final step occurring on-chip. To perform the assay, these researchers injected substrate into the channel to interact with the enzyme-linked antibody conjugated beads. They concentrated the fluorescent product downstream to achieve a 65-fold enhancement in signal in the presence of complex media, while demonstrating the ability to multiplex several concentrations at once for creation of a dose-response curve.[15] It should be noted that this protocol is limited by the large number of steps, which require skilled technicians. To address this limitation, Ko et al. increased throughput of the device up to 128 channels, with the capability of analyzing a series of concentrations ranging from 100- to 4000-fold enrichment simultaneously.[14] Deng et al. created a novel nanofluidic preconcentrator that leveraged a bubble valve for discrete localization of their antigen and capture beads, with a 4-fold improvement in LOD in the case of electrokinetic preconcentration.[13] However, all of these technologies are limited by their reliance on fluorescence for detection, which requires expensive or specialized equipment complicating its integration into POC diagnostics.

To create deliverable, equipment-free assays for POC sensing means a shift away from fluorescence detection to non-optical, label-free techniques all while maintaining high sensitivity. Sensale et al. created a non-optical membrane-based sensor for the detection of nucleic acid, protein, and endotoxin. As highly charged analytes bound the surface of the permselective membrane comprising the sensor, a shift in voltage for the onset of the overlimiting region in a current-voltage curve (CVC) taken across the membrane was observed. This shift in voltage was correlated to the target concentration. Their sensor exhibited constant underlimiting and limiting regions that served as a control for the assay. However, to perform their immunoassay, a detection antibody tagged with a charged nanoparticle was needed to produce a resolvable signal above background, due to the low net charge of proteins.[17]

Recent work from our group furthered this field with the development of a sensitive and selective, label-free sensor for nucleic acid detection at the surface of a packed microbead bed.[18] The device consists of a straight channel with two packed microbead beds: 1) the capturing region composed of streptavidin coated microbeads conjugated to biotinylated oligoprobes, and 2) the detection region with a 3D electrode composed of 15 μm-diameter Ag-coated glass beads overlying a Au thin-film microband. By application of an electrokinetic enrichment technique, faradaic ion concentration polarization (fICP), we observed enhanced hybridization of target DNA to the oligoprobe-conjugated microspheres. As the bound charge increased at the surface of the beads (due to hybridization), conduction of ions through the packed bed of bioconjugated beads to the 3D electrode was impacted, thereby producing a shift in current, which can be measured and used to quantify target concentration. The device has several advantages such as i) simple fabrication, ii) a non-optical, label-free sensing mechanism that does not require any specialized, bulky equipment and is therefore more amenable to POC implementation, and iii) high sensitivity

with picomolar detection limits for nucleic acid targets. However, over the concentration range employed, we noted target DNA hybridization occurred at a detectable level only after fICP focusing, and no significant signal was observed when performing the lateral flow assay alone (without enrichment).

In this paper, we have adapted the previous device architecture for a direct LFIA with label-free, non-optical detection of a weakly charged antigen with optional integration of electrokinetic preconcentration. Our results suggest that the detection mechanism is based on modulation of the surface conduction of ions along the surface of the bioconjugated beads upon antigen binding. We demonstrate the performance of this sensor using a model antigen, rabbit IgG, with and without an electrokinetic enrichment step. Binding of this protein target to a packed bed of bioconjugated microbeads leads to a shift in ionic current which can be measured at the 3D electrode. We demonstrate the shift in current occurs with a specific binding event, and with minimal signal in the presence of a non-specific (mismatched) target. This signal can be directly correlated to the concentration of antigen, and by fitting the linear portion of the curve an LOD of 31 nM was obtained for native (untagged) IgG. We investigate the device's ability to measure binding kinetics, with a rapid increase in signal after only two minutes and minimal signal drift over time. Finally, we implement an electrokinetic enrichment step, using fICP for a period of 40 min, to enhance the LOD by 84-fold and sensitivity by 4-fold. Control experiments utilizing fluorescently-tagged antigen indicate the fICP-LFIA incurs less loss of the antigen over time (flowed past the bioconjugated bead bed) when compared to the LFIA alone. These findings are important because they present a class of immunosensor that can directly detect weakly charged proteins without labelling or using optics. The device can be used for multiple interrogations of antigen to provide the signal at designated time points according to the user's needs. Depending on the clinically

relevant concentration range of the desired analyte, electrokinetic enrichment can be employed to help reach those limits-of-detection. Overall, the device has many advantages over existing technologies for POC testing including simple fabrication, automated readout, microliter sample sizes, rapid results, and picomolar sensitivity.

Experimental Section

Materials, Reagents, and Instrumentation. The antibodies, rabbit IgG isotype control Alexa Fluor 488 (Cat# 53-4616-82), rabbit IgG (H+L) secondary antibody (Cat# 65-6140), rabbit IgG isotype control (Cat# 14-4616-82), mouse IgG isotype control (Cat# 10400C), and mouse IgG (H+L) cross-adsorbed secondary antibody (Cat# 62-6540) were obtained from ThermoFisher Scientific (Waltham, MA). Pluronic F-127 was purchased from Sigma Aldrich (St. Louis, MO). All solutions were prepared using reagent grade chemicals (Fisher Scientific, Waltham, MA) and were diluted with double deionized water (18.2 MΩ·cm, Sartorius Arium Pro, Göttingen, Germany) to desired concentration. The running buffer was composed of 10 mM Tris·$HClO_4$ and 0.05% Tween-20.

For device fabrication, the following were purchased: poly(dimethylsiloxane) Sylgard 184 elastomer kit from Dow Corning Corp. (Midland, MI), SuperAvidin™ Coated Microspheres (d = 15.30 µm) from Bangs Laboratories (Fishers, IN), conductive Ag-coated hollow glass microspheres (d = 10-20 µm, 0.67 g/cc) from Cospheric (Santa Barbara, CA), and Au-coated glass slides with a Cr adhesion layer (1” x 3” x 0.40”; 50 Å Cr, 1,000 Å Au) from Evaporated Metal Films (Ithaca, NY). For slide development, the following were purchased: AZ 400K developer

(IMM) and chrome etchant (Sigma Aldrich, St. Louis, MO). For casting microchannels into PDMS, a Si wafer with SU-8 patterns was purchased (Custom Nanotech, Austin, TX).

Imaging and Data Processing. All images were obtained on an Eclipse Ti-S inverted fluorescence microscope from Nikon Industries (New York, NY) with a digital camera (Orca Flash 4.0) from Hamamatsu Corp. (Bridgewater, NJ). Fluorescence micrographs were obtained every 1 min for 60 min to monitor the local concentration of fluorescent tracers. Fluorescence image analysis was performed using ImageJ (National Institute of Health, Bethesda, MD). All fluorescence micrographs were background subtracted. Non-optical analysis was performed using custom designed circuit boards (InDesign, Indianapolis, IN) for current-voltage measurements. The analysis was also performed with a 6487 picoammeter/voltage source from Keithley (Cleveland, OH) with the current recorded by Keithley's ExceLINX software.

Coupling Biotinylated Capture Antibodies to Streptavidin-Coated Microspheres. Biotinylated goat anti-rabbit IgG was bound to streptavidin coated microspheres following the bead manufacturer's protocol (Bangs Laboratories, Fishers, IN). Briefly, 100 μL of the bead suspension was mixed with wash buffer (PBS, 0.05% Tween-20) at a 1:10 ratio. The beads were washed by centrifugation and the supernatant was discarded. This process was repeated two more times, before finally resuspending the beads to a concentration of 0.5 mg/mL in wash buffer. 10 μL of the biotinylated IgG was added to the bead solution and incubated for 30 min with gentle mixing at room temperature. Afterwards, the beads were washed to remove excess antibody, and then resuspended in the blocking buffer (1% BSA in PBS). The beads were then blocked at 4 ºC for at least 2 h. Finally, the bioconjugated beads were washed (3X) to remove the blocking buffer and replaced

with the storage buffer (10 mM Tris·$HClO_4$, 0.05% Tween-20, and 0.05% sodium azide) to a final volume of 100 μL, which was stored at 4 ºC for no more than 2 weeks.

Device Fabrication. The microfluidic device follows the same design that we previously described.[18] The Au electrodes were fabricated onto glass slides in a class 10/100 cleanroom using a standard published method.[19] Briefly, the Au coated glass slide with a Cr adhesion layer (5 nm) and Au top layer (100 nm) were spin coated with positive photoresist AZ P4620 and exposed to UV light through a photomask for 72 s. The exposed resist were developed with AZ 400K developer, and then the electrodes etched with 4% KI/ 1% I_2, chrome etchant, and washed with acetone to remove the photoresist. The Au electrode is then cleaned in a 1:1:1 (DDI water, NH_4OH, H_2O_2) base bath at 95 ºC for 1 h. The Au electrode was patterned as a microband with a width of 0.2 mm (and length exceeding the microchannel width) in the middle of the glass slide. Using the standard photolithographic process[20] the glass slide was irreversibly bound to a PDMS layer embedded with a main channel (40 μm tall, 11.0 mm long, and 1.48 mm wide) containing two bead beds defined by rows of 20 μm-wide retaining posts with 10 μm gaps between. The primary bead bed (300 μm long, for Ag beads) and the bioconjugated bead bed (500 μm long, for SuperAvidin™ Coated Microspheres). The two bead beds were accessed by packing channels (200 μm wide and 2.5 mm long). The packing channel inlets and the outlet of the main channel were created using a 1.0 mm-diameter biopsy punch, and a 3.0 mm-diameter biopsy punch was used to create the inlet of the main channel. The glass slide with microband electrode and PDMS slab were irreversibly bound by first, exposure to air plasma (PDC-001, Harrick Plasma, Ithaca, NY) for 60 s, then alignment and placing them in contact, and finally, baking at 65 ºC for 24 h.

To minimize non-specific binding on the channel walls, the device was filled with 3.0 μM Pluronic solution and stored overnight. The device was rinsed thoroughly with DDI before preparation of the bead beds. The primary bead bed was packed with a suspension of Ag beads in DDI water using a pipette and was sealed using PDMS precursor injected by needle. The device was baked at 65 ºC for 2 h to ensure that the PDMS was cured. The device was evacuated under vacuum for 15 min prior to filling the bioconjugated bead bed to help facilitate packing. The device was sealed with PDMS and left at room temperature for 24 h. Prior to using the device, the 1 mm O.D. stainless steel driving electrodes connected the inlet and outlet of each device and copper tape was attached to the Au electrode.

Non-optical detection and analysis of IgG in the LFIA. First, the device was evacuated under vacuum for 15 min and then filled with running buffer. Second, the device was rinsed for 1 h at 500 nL/min with running buffer. Third, the device was conditioned by applying 3.0 V between the leads in the inlet and outlet versus ground at the 3D electrode for 5 min. Fourth, the flow rate was decreased to 100 nL/min and three current voltage curves (CVCs) were conducted 5 min apart. Each CVC was obtained from 0 V to 5.5 V in 0.25 V increments at a rate of 0.33 s per step. Fifth, the buffer was replaced with the analyte solution, which is placed in the inlet reservoir and flowed in at 100 nL/min with CVCs taken 5 min apart for 1 h. To account for variability in device packing, the average of the first three CVCs obtained in the presence of buffer solution only was subtracted from each CVC taken after the analyte was added to the inlet.

Evaluation of IgG Species Electrokinetic Enrichment by fICP. First, the device was evacuated under vacuum for 15 min and then with the running buffer. Second, the device was rinsed for 1 h

at 500 nL/min and, third, conditioned at 3.0 V for 5 min. Fourth, the flow rate was decreased to 100 nL/min and three current voltage curves (CVCs) were taken 5 min apart (each 0 V to 5.5 V in 0.25 V increments at a rate of 0.33 s per step). Fifth, following the last CVC of the buffer solution, a background fluorescence image was obtained. Sixth, the buffer was replaced with the analyte solution which was placed in the inlet reservoir and flowed in at 100 nL/min for 5 min before the application of voltage, to ensure the analyte had reached the bead bed. To preconcentrate the analyte over the bioconjugated bead bed, 9.0 V was applied (at the inlet/outlet leads versus ground at the 3D electrode) for 40 min. The voltage was then turned off and the device was rinsed for 5 min to remove any unbound analyte. After this period, a final CVC was recorded. To account for variability in device packing, the average of the first three CVCs from the buffer solution was subtracted from the CVC taken after enrichment.

Results and Discussion

Device design and label-free sensing mechanism. Scheme 1A shows the circuit including the device and an example of the resulting current-voltage curve (CVC) measured electronically. Two positive leads are attached to the inlet and outlet and the 3D electrode is grounded. In order to account for device-to-device variability, CVCs are obtained in the presence of running buffer alone before the addition of analyte and then averaged. The CVC representing buffer only is then subtracted from the CVC obtained in the presence of analyte, resulting in a shift in current as a function of voltage, or "CVC shift". The basic principle of our on-chip, bead-based lateral flow immunoassay (LFIA) is shown in Scheme 1B. Initially, before addition of sample, the bioconjugated bead bed is composed of biotinylated capture antibody coated on streptavidin

microbeads. Following the addition of the target antigen, rabbit IgG, to the inlet, the capture antibody, goat anti-rabbit IgG, binds the target. Antigen therefore accumulates (is bound) at the bioconjugated bead bed (dark gray) where it can later be sensed by a change in ionic current (across the packed bed of bioconjugated beads) measured by the 3D electrode (light gray). A top view brightfield micrograph exhibiting the two packed microbeads is shown in Figure 1A.

To aid in illustrating the sensing mechanism, an equivalent circuit approximating the resistance in each device segment is given in Scheme 1C. The total resistance on-chip (R_{tot}) is composed of the channel resistance (R_{Ch1} and R_{Ch2}), the resistance through the bead bed with two resistive paths: resistance of the bulk solution (R_B) and resistance to the conduction of ions across the surface of the bioconjugated beads (R_S), and finally, the resistance to charge transfer (R_{CT}) at the electrodes. Previous studies have shown that R_S is a major contributor to R_{tot}.[18] This feature is important because as R_S is modulated by changes in the bead surface, the measured current is significantly impacted and thus, can be used as a means of sensing. For the case of protein-protein interactions, and previously with nucleic acid interactions, a positive shift in current is observed after binding or hybridization occurs. A more detailed exploration of the device mechanism can be found in Scheme 1D. As the fixed negative charge on the surface of the bioconjugated beads is increased (i.e., by the binding of antigen to antibody), the zeta potential, which is negative, and concentration of mobile charges in the electrical double layer (EDL) increase, thereby increasing the surface conductance. In other words, cations accumulate in the EDL and are conducted at a greater rate across the surface of the beads, towards the 3D electrode. As this surface conductance increases, R_s decreases, and the total current through the device increases. The resulting current signal can be directly related to the presence of antigen bound on the bioconjugated microbeads and to the corresponding sample concentration. In addition to the charge of the analyte, increases

in surface area and changes in charge distribution on the bead surface may also impact the surface conductance. This sensing mechanism is applied to the following experiments to achieve label-free detection of antigen-antibody binding events.

Non-optical detection of a lateral flow immunoassay via ion conduction. To investigate binding between the antigen and the bioconjugated microbeads, experiments tracking the spatial distribution of fluorescently tagged IgG were carried out. The target analyte, 10 nM rabbit IgG-Alexa Fluor (AF) 488, was introduced and monitored for a period of 50 min at the location of the bioconjugated bead bed. Figure 1B shows the resulting fluorescence micrographs of the LFIA taken at t = 1 min and t = 50 min, where an increase in fluorescence over the bioconjugated bead

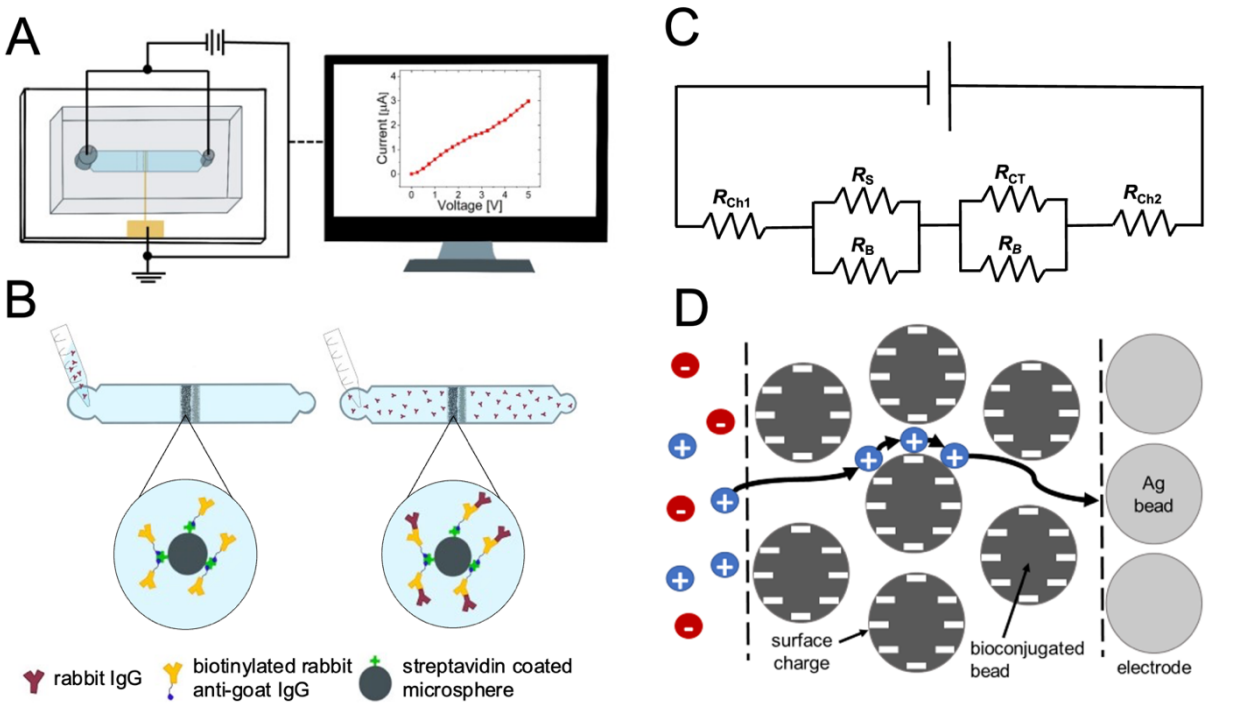

Scheme 1. Schematic overview of the bead-based lateral flow immunoassay and mechanism of label-free electrochemical detection. (A) Workflow of device, from applied voltage to electronically measured current measurements. (B) Sequential steps of the on-chip LFIA. (C) Resistance variables of device circuit ($V_{tot} = i_{tot}R_{tot}$). (D) Mechanism for label-free electrochemical detection of antigen-antibody binding events.

bed was observed at the end of the assay. The analysis of the average fluorescence intensity over this bead bed as a function of time revealed a rapid increase after only 3 min. The rising signal eventually plateaued at 50 min (Figure 1C). To obtain this intensity profile, a region of interest was drawn over the bioconjugated bead bed, the average intensity was measured, and the background was subtracted using the signal obtained when the device was filled with buffer only.

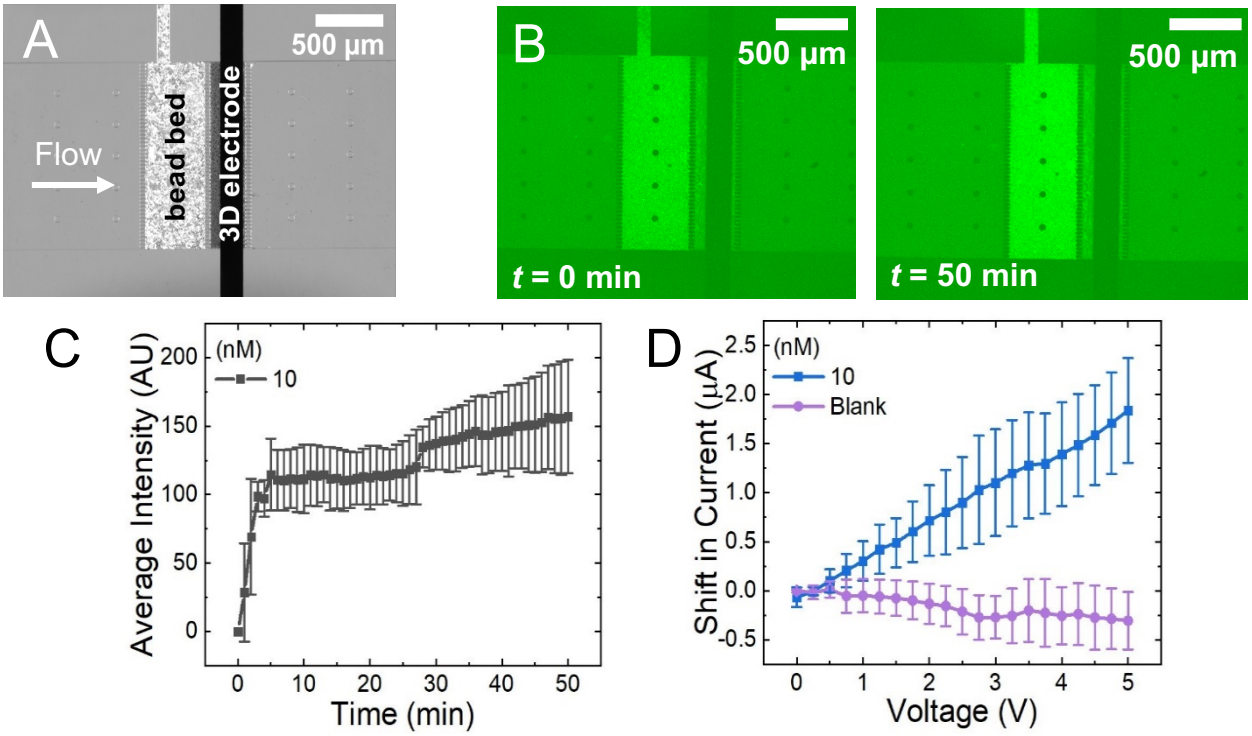

Figure 1. Binding of 10 nM rabbit IgG- AF 488 (10 mM Tris•$HClO_4$, 0.05% Tween-20, pH 8.3) to the bioconjugated bead bed during the on-chip LFIA. (A) Brightfield micrograph of device which consists of a singular microfluidic channel with a two bead bed system: the first, streptavidin coated microbeads conjugated to biotinylated goat anti-rabbit IgG, and the second, a 3D electrode composed of 15 µm Ag beads packed over a Au electrode. (B) Fluorescence micrographs taken after the addition of antigen (10 nM rabbit IgG-AF 488) at t = 1 min and t = 50 min. (C) Plot of fluorescence intensity data of the LFIA (n = 3). The average intensity was measured over the area of the bioconjugated bead bed and background subtracted. Intensity values were recorded every 1 min. (D) Plot of shift in current as a function of voltage for IgG-AF 488 (blue trace) and the blank (purple trace). The current was measured at t = 50 min (n = 7) and buffer subtracted to produce the shift in current.

These results confirmed the binding of IgG-AF 488 at this test line.

Next, we evaluated the impact that binding of the protein target has on the current. The shift in current as a function of voltage was compared for 10 nM IgG-AF 488 and a blank at t = 50 min (Figure 1D). At t = 0 the antigen was added to the inlet and the current was monitored every

5 min. After completion of the assay, IgG-AF 488 (blue trace) yielded a much larger signal of nearly 1.8 μA (at 5.0 V) when contrasted with the blank (running buffer, purple trace), which had a shift of -0.3 μA. We determined CVC shifts for a series of concentrations of IgG-AF 488 at 5.0 V where the resulting signal was resolved from the blank (Figure S1). Higher concentrations of antigen were correlated to higher shifts in current. The calibration curve and determined LOD of 3 nM for IgG-AF 488 can be found in the *Supporting Information* (*SI*, Figure S2). The CVC shift and features of the calibration curve are discussed in greater detail for the unlabeled antigen (in the absence of fluorescent dye) in the following subsection. These results indicate that the hybridization of a protein target to the antibody-coated microbeads produces a measureable shift in ionic current that can be leveraged for label-free detection of antigen-antibody binding events.

Quantitative determination of label-free IgG. To rule out interference of the charged dye label used in the experiments described in the previous subsection, we moved to a label-free analyte, native (untagged) rabbit IgG. This change ensured that all charge accumulated at the surface of the bead-based test line and the resulting shift in current could be attributed to the protein only. We devised these experiments for a direct LFIA where the antigen signal is measured after being bound at the surface, without a detector antibody or fluorescent label. Figure 2A compares the shift in current obtained for 500 nM target IgG to the blank signal. At 5.0 V, after 50 min, the protein target (red trace) produced a signal of approximately 19 μA (at 5.0 V) whereas the blank (running buffer, purple trace) generated a small negative shift of -0.3 μA. The large shift in current created by the target can be attributed to its binding by the capture antibodies at the bioconjugated bead bed. These results reveal that even a weakly charged target, such as a protein, contributes to the

change in surface conductance in the sensor and thereby, influences the current after subsequent binding.

To evaluate the selectivity and specificity of the sensor, we introduced a non-target analyte, mouse IgG, at the same concentration of 500 nM as the target analyte, rabbit IgG (Figure 2A). The shift in current generated by the non-target corresponded to 3 μA which was much smaller than the target's shift of 19 μA. When expressed as a signal-to-noise ratio, a value of approximately 6.3 is obtained. We conclude that the detected shift in current occurs with a specific binding event in the LFIA, as a minimal signal was produced in the presence of a non-specific analyte. While some non-specific binding does occur on-chip, future studies will be focused on determining the best pretreatment procedure to ensure higher specificity.

We next investigated the relationship between the concentration of antigen and the resulting signal. Figure 2B shows the shift in current as a function of voltage for a series of concentrations of the protein target. Similar to previous results, higher concentrations produced a larger shift in current than lower concentrations of the same antigen. To construct our calibration curve, we selected the signal at 5.0 V as each CVC shift was clearly resolved from one another at that specific voltage. The calibration curve compared the shift in current at t = 50 min to the corresponding concentration (Figure 2C). The calibration curve was fitted to a Langmuir curve with an R^2 value of 0.9856 showing good agreement between the experimental results and predicted fitting. The linear portion of the calibration curve was then fitted and the resulting linear line equation was used in determining the LOD. The lowest concentration, 50 nM IgG, was measured seven times to obtain the standard deviation which was multiplied by three and added to the signal of the blank. The LOD for target IgG was found to be 31 nM with a sensitivity of 0.0377

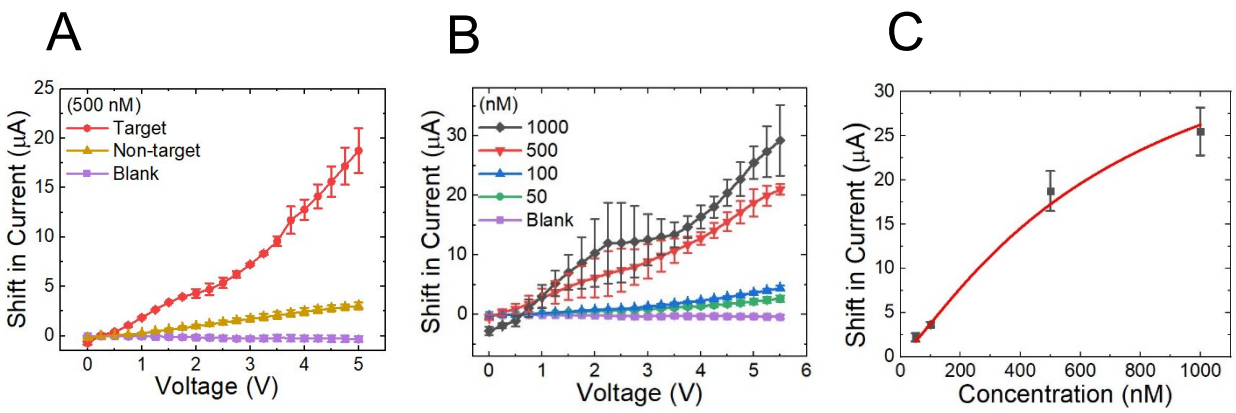

Figure 2. Label-free detection of untagged rabbit IgG (10 mM Tris•$HClO_4$, 0.05% Tween-20, pH 8.3) following the on-chip LFIA. All CVCs were measured at t = 50 min ($n \geq 3$). (A) Plot of CVC shift showing the signal produced for the target, rabbit IgG (red trace), non-target, mouse IgG (gold trace), and blank (purple trace). (B) Plot of CVC shifts for a series of distinct concentrations of rabbit IgG (0 nM purple, 50 nM green, 100 nM blue, 500 nM red, and 1000 nM black). (C) Calibration curve obtained for the on-chip LFIA ($n \geq 3$) at t = 50 min. A Langmuir fitting yielded an R^2 value of 0.9856. The LOD was calculated by fitting the linear portion of the curve to find the IgG concentration corresponding to the signal of the blank + 3 SD (50 nM, n = 7).

μA/nM. This value is higher than the determined LOD for IgG-AF 488, which we hypothesize is due to the impact of the charged fluorescent dye on current and possibly on binding.

While this LOD can be improved, especially when compared to other reported values in the literature, these results are significant because this method employs a label-free sensing mechanism for protein hybridization and directly relates it to concentration of antigen for quantitative analysis. This LOD is expected to improve following optimization of several parameters such as bead bed length, microbead diameter, and buffer concentration and identity. Finally, the present sensing scheme follows a direct LFIA where the antigen signal is measured without a detector antibody. However, the results of the previous subsection suggest that incorporation of a label or a tagged secondary antibody may improve the LOD, because the addition of charge (or surface area) to the system would compensate for the target's inherently low charge. Improvement of the LOD by electrokinetic pre-enrichment of the analyte is discussed below in the subsection *Integration of fICP with the LFIA*.

Characterization of antigen-antibody binding kinetics on-chip. We next investigated the binding kinetics of IgG through our platform by measuring the observed signal through time. First, the device was filled with 1000 nM IgG at $t = 0$. Then, CVCs were obtained once every 1 min until $t = 20$ min. In the meantime, the solution in the inlet was replaced with buffer at $t = 10$ min (Figure 3A). A rapid increase in signal was observed after only 2 min due to binding of the target antigen by the capture antibody, and an eventual plateau in signal occurred at approximately 20 μA due to achieving equilibrium coverage (binding site occupancy) at the test line. When the antigen was removed and replaced with buffer only, we observed an exponential decrease in signal attributed to a shift in equilibrium binding towards the unbound state. This signal eventually returned to a baseline near 3 μA. This result is significant because it shows that this device can be utilized to study binding kinetics. A key point is that this signal can be used to monitor changes in antigen concentration over time (not just a single time point).

We evaluated shift in current as a function of time for several concentrations, as shown in Figure 3B (Figure S3a is a zoomed-in version comparing the lowest concentration and the blank). Similar to previous results, we observed higher concentrations of analyte yielding higher shifts in

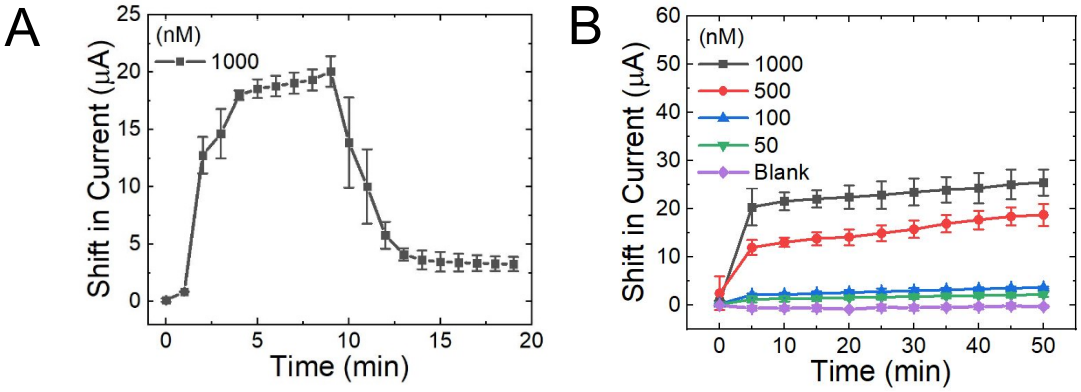

Figure 3. Binding kinetics and mass transport characterized on-chip for target IgG (10 mM Tris•$HClO_4$, 0.05% Tween-20, pH 8.3). All current measurements were taken at 5.0 V ($n \geq 3$). (A) Plot of shift in current versus time after the addition of 1000 nM IgG at $t = 0$, and the replacement of IgG with buffer before $t = 10$ min. (B) Plot of shift in current versus time for five concentrations of IgG (0 nM purple diamonds, 50 nM green inverted triangles, 100 nM blue triangles, 500 nM red circles, and 1000 nM black squares).

current when compared to lower concentrations, with minimal drift after a period of 50 min. Interestingly, we noted that higher concentrations of antigen reaching a plateau in signal faster than lower concentrations (see Figure S3a). This same phenomenon has been previously reported in the literature for other non-optical sensors, as higher concentrations of ligand are able to reach equilibrium coverage more quickly.[21] A detailed comparison for the binding kinetics of target and non-target IgG can be found in the *Supporting Information* (*SI*, Figure S3b).

Based on these results, we anticipate the proposed method can be used to determine kinetic parameters for any antigen-antibody interaction. While surface plasmon resonance (SPR) is used extensively to measure affinity and binding kinetics for specific ligands, it relies on optical equipment to operate. The device presented here provides a non-optical route to explore the rate of association and dissociation between an antigen and antibody.

Integration of fICP with the LFIA. In order to improve detection limits of IgG sensing, we incorporated an initial electrokinetic preconcentration step, using fICP, before readout. Scheme 2 shows how fICP is used within our device to preconcentrate an anionic analyte over the bioconjugated bead bed. We describe the fICP mechanism in our device briefly. First, the channel is filled with an electrolyte solution that is distributed evenly throughout the entire channel, and continuous fluid flow is established (left to right, Scheme 2A). When voltage is applied, water reduction occurs at the cathode (grounded microband, Scheme 2B) producing hydroxide which reacts with the $TrisH^+$ present in the electrolyte to produce a neutral species (Tris) within the primary (Ag) bead bed. As ions have been consumed from this area, we refer to it as the ion depletion zone (IDZ). The IDZ extends downstream by fluid flow. Within the IDZ, there is low ionic conductivity, which results in high resistivity. By Ohm's law, a steep electric field gradient

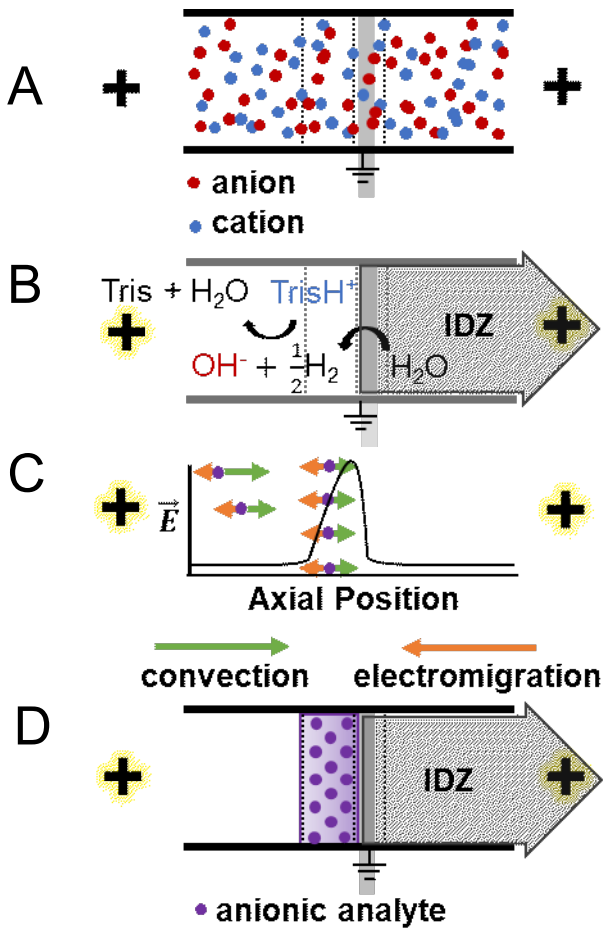

Scheme 2. A schematic overview of the mechanism for faradaic ion concentration polarization as it occurs in the device.

forms at the boundary of the IDZ (Scheme 2C). The anionic analyte is attracted towards the anodes on either end of the microfluidic device by electrophoresis (orange arrows, Scheme 2C). Convective forces (purple arrows, Scheme 2C) consisting of electroosmotic flow and pressure induced flow carry the anionic analyte from the inlet towards the bioconjugated bead bed. The analyte focuses at an axial location along the electric field gradient where its convective and electromigratory velocities are equal and opposite (Scheme 2C). By this method, charged analytes can be preconcentrated into a stable focused plug at a precise location, in this case over the bioconjugated bead bed (Scheme 2D).

The details of the experiments, in which fICP focusing was used, are as follows. After the addition of the target (10 nM IgG-AF 488) at t = 0 min, the device was incubated for 5 min with constant flow before the application of 9.0 V to induce fICP. Using this fluorescently labeled IgG, we were able to track the enrichment of the protein at distinct voltages (7.0, 8.0, 9.0, and 10 V). We observed bursting (escape over the IDZ and washing downstream) of the enriched plug at 7.0 and 8.0 V. At 10 V, we noted severe bubble formation downstream of the bead bed occurring at later times (>10 min) in the experiment. For these reasons, we selected 9.0 V where minimal bursting and rare bubble formation was noted. Figure 4 shows the fluorescence micrographs of the device before, during, and after the enrichment of IgG-AF 488. The voltage was applied for a total of 40 min and turned off before performing a wash for a period of 5 min to ensure any unbound analyte was removed. Finally, at t = 50 min, a CVC was recorded to determine the signal of the fICP-LFIA for later comparison to the LFIA only.

Using this protocol with unlabeled IgG, we evaluated the impact of electrokinetic enrichment on the specificity of the sensor. Figure 5A shows the CVC shifts obtained for 100 nM target (rabbit IgG) and non-target (mouse IgG) as well as the blank following fICP-driven enrichment. Notably, the target and non-target IgG were both unlabeled, so that all charge in the system can be attributed to these proteins only. At 5.0 V, the shift for the non-target IgG at 100 nM is similar to the signal of the target at 10 nM, and thus, the specific signal is 10 times higher than the non-specific signal, at the same concentration. These results confirmed that the enhancement in signal following fICP focusing was due to specific binding of the antigen.

We next evaluated the CVC shifts for a series of concentrations ranging from 0.1-100 nM for rabbit IgG following fICP-driven enrichment (Figure 5B). As before, we observed higher shifts in signal correlated to higher starting concentrations of analyte. We were unable to perform experiments with concentrations higher than 100 nM due to bubble formation downstream of the primary (Ag) bead bed due to increased current, which occurred only at high concentrations of target. It is important to note this effect was not observed at lower concentrations. We then plotted the shift in current (at 5.0 V) as a function of concentration to obtain the calibration curve for the fICP-LFIA (Figure 5C). A Langmuir fitting was used for the data set with an R^2 value of 0.9993

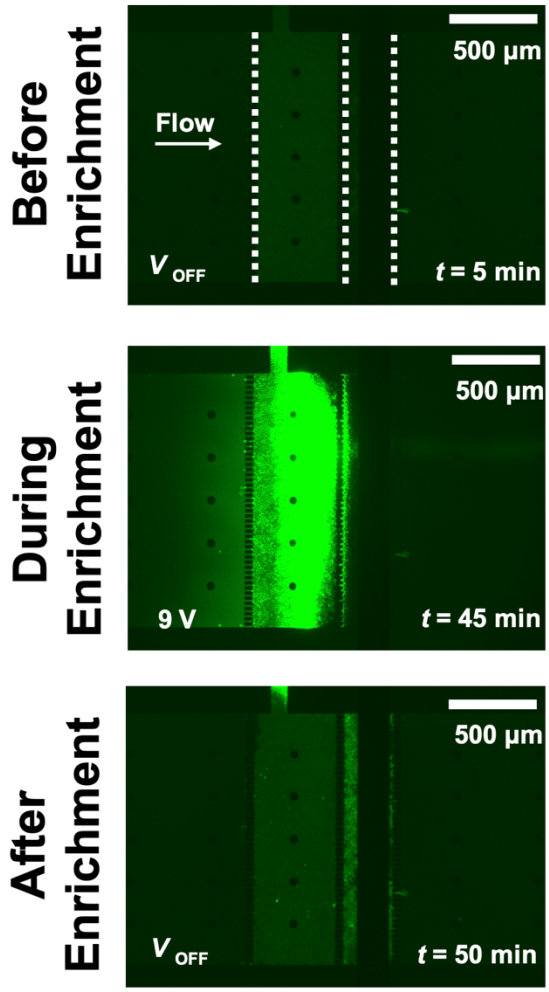

Figure 4. Fluorescence micrographs taken of the integrated fICP-LFIA experiment showing before, during, and after electrokinetic enrichment. To visualize fluorescence, 10 nM rabbit IgG-AF 488 (10 mM Tris•$HClO_4$, 0.05% Tween-20, pH 8.3) was added to the device inlet. To perform fICP, 9.0 V was applied from t = 5 min to t = 45 min.

indicating excellent agreement between the observed and predicted values. We applied a linear fitting to the linear portion of the curve to find the LOD. We determined the LOD for the fICP-LFIA was 370 pM, which was an 84-fold improvement when compared to the LFIA only. By implementing fICP, we were able to bring detection limits within the picomolar range, which is comparable to other label-free immunosensors reported in the literature (Table S1). Based on the slope of the calibration curve, the sensitivity was 0.1505 μA/nM, an increase of 4-fold versus LFIA only. The importance of these results is that this platform can be made much more sensitive for protein sensing by simply incorporating the initial electrokinetic step. This step can be optimized for preconcentration of any anionic analyte, which encompasses many biological targets. While ICP has been shown extensively in conjunction with immunoassays, to the best of our knowledge, this paper reports the first non-optical detection of a concentration polarization enhanced bead-based LFIA.

To further elucidate the mechanism of signal enhancement, we performed experiments using fluorescently labelled IgG to compare the amount bound to the test line (bioconjugated

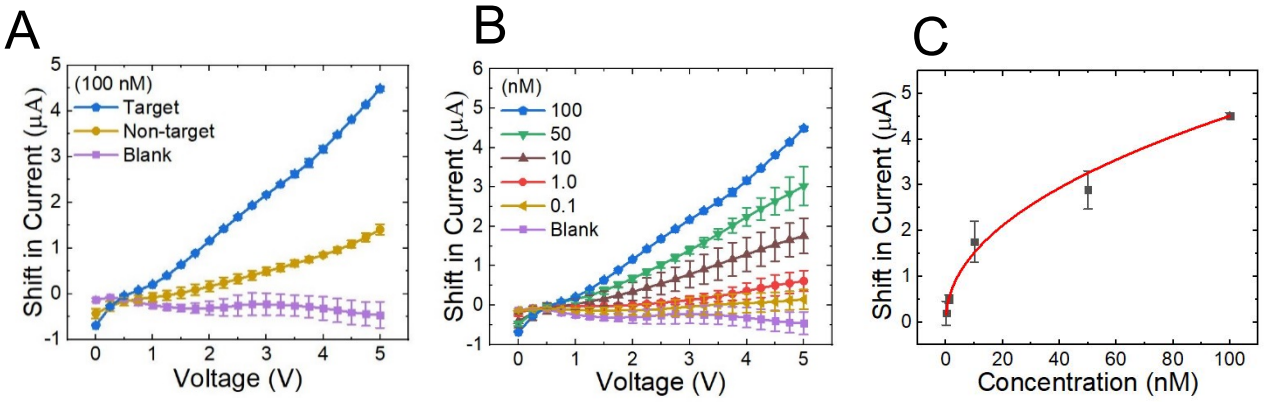

Figure 5. fICP focusing of rabbit IgG (10 mM Tris•$HClO_4$, 0.05% Tween-20, pH 8.3) at 9.0 V directly over the bioconugated bead bed. CVCs were measured at 5.0 V and t = 50 min ($n \geq 3$). (A) Plot of CVC shifts after electrokinetic enrichment of target antigen, rabbit IgG (blue trace), and non-target, mouse IgG (gold trace), compared to the blank (purple trace). (B) Plot of shift in current as a function of voltage for six concentrations of IgG (0 nM purple, 0.1 nM gold, 1 nM red, 10 nM brown, 50 nM green, 100 nM blue) obtained after electrokinetic enrichment. 9.0 V was applied from t = 5 min to t = 45 min. (C) Calibration curve generated for the fICP-LFIA. The calibration curve was fit to a Langmuir curve with an R^2 value of 0.9993. The LOD was calculated by fitting the linear portion of the curve to find the IgG concentration corresponding to the signal of the blank + 3 SD (100 pM, n = 7).

beads) and percent loss (the fraction carried downstream of the test line) among three cases: LFIA only, fICP only, and the fICP-LFIA. The LFIA was previously described in an earlier section where IgG-AF 488 was flowed through the channel for 50 min and bound at the bioconjugated bead bed. To investigate the effects of fICP only, we used streptavidin microbeads that were not conjugated with a capture antibody. We then performed preconcentration of IgG-AF 488 from t = 5 min to t = 45 min, with a total assay time of 50 min. The fICP-LFIA followed the same procedure, but included capture antibody bound at the bioconjugated bead bed. All obtained fluorescence micrographs were background subtracted during subsequent analysis.

Figure S4 shows the average intensity of IgG-AF 488 at the test line as a function of time for all three cases. Specifically, this average intensity was measured over a region of interest encompassing the bioconjugated bead bed every 1 min for a period of 50 min. The results indicated that, throughout the duration of the assay, the fICP-LFIA had the highest average intensity, followed by the fICP only case, and finally, the LFIA. Based on these results, we conclude that both electrokinetic enrichment and specific binding contribute to the signal obtained for the fICP-LFIA, and we hypothesize that these mechanisms work in concert to prevent loss of the analyte (washing past the test line). These conclusions are further supported by considering the calculated maximum enrichment factor, which was 500x for the fICP-LFIA, compared to 300x for fICP only, and 2.5x for the LFIA. The maximum enrichment factor was determined by selecting the highest average intensity measured over the bioconjugated bead bed and dividing by the initial average intensity. We defined the initial intensity using the data collected from the fICP only case to account for any binding that occurs during the LFIA or fICP-LFIA.

We then investigated the percent loss of analyte as a function of time for all three cases (Figure S5). Here percent loss of the analyte is defined as the fraction of the analyte (IgG) that

washes past the test line, and it is calculated as the average intensity downstream of the microbead beds divided by the initial intensity, multiplied by a factor of 100. This factor was monitored over the full duration of the experiment. By finding the area under each curve, we determined the fICP-LFIA retains 37.8% more IgG than the LFIA alone. These results support the enhancement in LOD observed when electrokinetic enrichment is interfaced with a bead-based immunoassay.

Conclusions

In this study, we have reported several key advancements in the field of protein sensing. First, we have presented a simple device leveraging an ion conduction sensing mechanism with the ability to non-optically detect weakly charged analytes, such as proteins, directly. Other non-optical sensors reported in the literature needed highly charged reporters to yield a signal in the presence of target proteins. Performing our on-chip LFIA is reagent-free and requires minimal manual intervention by using automated electronic readout. We have demonstrated a wide application of the described non-optical, label-free sensing mechanism, such as the ability to characterize the binding kinetics of antigen-antibody pairs, which typically requires fluorescence microscopy or SPR for detection. Second, we implemented an initial electrokinetic preconcentration step to focus target antigen directly over the bead-based test line. We found the fICP-LFIA can improve the LOD for these types of assays. Whereas other reported electrokinetically enhanced immunoassays have used fluorescence detection, we leverage a label-free ion conduction sensing scheme to detect the specific binding of targets after preconcentration. Together, these findings establish a sensitive platform for performing LFIAs without the use of microscopy or other bulky, external equipment. An important advantage of this device is its versatility, as it can be tuned to recognize other protein-

protein interactions, and has already been established for nucleic acid sensing. We envision this device can be used either qualitatively to detect a biomarker for diagnostic purposes, or quantitatively to ascertain disease progression by days or measure a patient's immune response. Currently, our laboratory is investigating other antigens for sensing of highly infectious disease and implementing thermoplastic microchips in lieu of PDMS/glass devices to enable mass production for POC application.

Associated Content

Supporting Information

The Supporting Information including current-time curves recorded for IgG-AF 488, a calibration curve for IgG-AF 488, a comparison of current-time curves between the blank, target, and non-target analyte, a table comparing the performance of label-free immunosensors, and fluorescence data used to calculate the average intensity and percent loss in LFIA-fICP, fICP only, and LFIA only cases, is available free of charge at …

Author Information

Corresponding Author

Robbyn K. Anand — *Department of Chemistry, Iowa State University, Ames, Iowa 50011, United States;*

Email: rkanand@iastate.edu

Authors

Sommer Osman — *Department of Chemistry, Iowa State University, Ames, Iowa 50011, United States*

Echo L. Claus — *Department of Chemistry, Iowa State University, Ames, Iowa 50011, United States*

Notes

The authors declare no competing financial interest.

Acknowledgements

This work has been supported by the Roy J. Carver Charitable Trust through award number 21-5449 and an NSF CAREER grant awarded by the Chemistry Directorate Chemical Measurement and Imaging Program under award number 1849109.

References

(1) Everitt, M. L.; Tillery, A.; David, M. G.; Singh, N.; Borison, A.; White, I. M. A Critical Review of Point-of-Care Diagnostic Technologies to Combat Viral Pandemics. *Anal. Chim. Acta* **2021**, *1146*, 184–199. https://doi.org/10.1016/j.aca.2020.10.009.

(2) Manmana, Y.; Kubo, T.; Otsuka, K. Recent Developments of Point-of-Care (POC) Testing Platform for Biomolecules. *TrAC - Trends Anal. Chem.* **2021**, *135*, 116160. https://doi.org/10.1016/j.trac.2020.116160.

(3) Murray, L. P.; Mace, C. R. Usability as a Guiding Principle for the Design of Paper-Based, Point-of-Care Devices – A Review. *Anal. Chim. Acta* **2020**, *1140*, 236–249. https://doi.org/10.1016/j.aca.2020.09.063.

(4) Gubala, V.; Harris, L. F.; Ricco, A. J.; Tan, M. X.; Williams, D. E. Point of Care Diagnostics : Status and Future. **2012**, *84* (2), 487–515. https://doi.org/https://doi.org/10.1021/ac2030199.

(5) Ng, A. H. C.; Uddayasankar, U.; Wheeler, A. R. Immunoassays in Microfluidic Systems. *Anal. Bioanal. Chem.* **2010**, *397* (3), 991–1007. https://doi.org/10.1007/s00216-010-3678-8.

(6) Wang, Y. C.; Han, J. Pre-Binding Dynamic Range and Sensitivity Enhancement for

Immuno-Sensors Using Nanofluidic Preconcentrator. *Lab Chip* **2008**, *8* (3), 392–394. https://doi.org/10.1039/b717220f.

(7) Berzina, B.; Anand, R. K. Tutorial Review: Enrichment and Separation of Neutral and Charged Species by Ion Concentration Polarization Focusing. *Anal. Chim. Acta* **2020**, *1128*, 149–173. https://doi.org/10.1016/j.aca.2020.06.021.

(8) Krishnamurthy, A.; Anand, R. K. Recent Advances in Microscale Extraction Driven by Ion Concentration Polarization. *TrAC - Trends Anal. Chem.* **2022**, *148*, 116537. https://doi.org/10.1016/j.trac.2022.116537.

(9) Moghadam, B. Y.; Connelly, K. T.; Posner, J. D. Two Orders of Magnitude Improvement in Detection Limit of Lateral Flow Assays Using Isotachophoresis. *Anal. Chem.* **2015**, *87* (2), 1009–1017. https://doi.org/10.1021/ac504552r.

(10) Kim, C.; Yoo, Y. K.; Han, S. Il; Lee, J.; Lee, D.; Lee, K.; Hwang, K. S.; Lee, K. H.; Chung, S.; Lee, J. H. Battery Operated Preconcentration-Assisted Lateral Flow Assay. *Lab Chip* **2017**, *17* (14), 2451–2458. https://doi.org/10.1039/c7lc00036g.

(11) Park, S.; Yossifon, G. Combining Dielectrophoresis and Concentration Polarization-Based Preconcentration to Enhance Bead-Based Immunoassay Sensitivity. *Nanoscale* **2019**, *11* (19), 9436–9443. https://doi.org/10.1039/c9nr02506e.

(12) Lu, B.; Maharbiz, M. M. Ion Concentration Polarization (ICP) of Proteins at Silicon Micropillar Nanogaps. *PLoS One* **2019**, *14* (11), 1–17. https://doi.org/10.1371/journal.pone.0223732.

(13) Deng, C. Z.; Fan, Y. J.; Chung, P. S.; Sheen, H. J. A Novel Thermal Bubble Valve Integrated Nanofluidic Preconcentrator for Highly Sensitive Biomarker Detection. *ACS Sensors* **2018**, *3* (7), 1409–1415. https://doi.org/10.1021/acssensors.8b00323.

(14) Ko, S. H.; Kim, S. J.; Cheow, L. F.; Li, L. D.; Kang, K. H.; Han, J. Massively Parallel Concentration Device for Multiplexed Immunoassays. *Lab Chip* **2011**, *11* (7), 1351–1358. https://doi.org/10.1039/c0lc00349b.

(15) Cheow, L. F.; Ko, S. H.; Kim, S. J.; Kang, K. H.; Han, J. Increasing the Sensitivity of Enzyme-Linked Immunosorbent Assay Using Multiplexed Electrokinetic Concentrator. *Anal. Chem.* **2010**, *82* (8), 3383–3388. https://doi.org/10.1021/ac9024335.

(16) Li, M.; Anand, R. K. Recent Advancements in Ion Concentration Polarization. *Analyst* **2016**, *141* (12), 3496–3510. https://doi.org/10.1039/c6an00194g.

(17) Sensale, S.; Ramshani, Z.; Senapati, S.; Chang, H. C. Universal Features of Non-Equilibrium Ionic Currents through Perm-Selective Membranes: Gating by Charged Nanoparticles/Macromolecules for Robust Biosensing Applications. *J. Phys. Chem. B* **2021**, *125* (7), 1906–1915. https://doi.org/10.1021/acs.jpcb.0c09916.

(18) Berzina, B.; Peramune, U.; Claus, E. L.; Kim, S.; Saurabh, K.; Strait, M. E.; Ganapathysubramanian, B.; Anand, R. K. Electrokinetic Enrichment and Electrical Detection of Nucleic Acids by Conduction of Ions Along the Surface of Bioconjugated Beads for Point-of-Care Testing. **2022**, *To be submitted*.

(19) Xia, Y.; Whitesides, G. M. SOFT LITHOGRAPHY. *Annu. Rev. Mater. Sci* **1998**, *28* (1), 153–184. https://doi.org/https://doi.org/10.1146/annurev.matsci.28.1.153.

(20) Dertinger, S. K. W.; Chiu, D. T.; Noo Li Jeon; Whitesides, G. M. Generation of Gradients Having Complex Shapes Using Microfluidic Networks. *Anal. Chem.* **2001**, *73* (6), 1240–1246. https://doi.org/10.1021/ac001132d.

(21) Cui, W.; Zhao, P.; Wang, J.; Qin, N.; Ho, E. A.; Ren, C. L. Reagent Free Detection of SARS-CoV-2 Using an Antibody-Based Microwave Sensor in a Microfluidic Platform.

Lab Chip **2022**, *22*, 2307–2314. https://doi.org/10.1039/d2lc00145d.